STRUCTURAL AND MAGNETIC PROPERTIES IN THE DIMER LATTICE $Ba_8NdRu_4Br_2O_{18}$

by

Elliot Roberts
Department of Physics

Gang Cao, Thesis Advisor, Department of Physics
Paul Beale, Honors Council Representative, Department of Physics
Ellen Broering, Outside Reader, Department of Chemistry

A thesis submitted in partial fulfillment of the requirements
for the degree of BA with Honors

Professor Gang Cao Research Group
University of Colorado Boulder

Defense Date: 4 April 2023

Abstract

This paper will present magnetic and structural data for the dimer lattice $Ba_8NdRu_4Br_2O_{18}$ and attempt to understand the findings using a theoretical model. This paper will preface the analyzation of data with a theoretical background that is designed to motivate and aid in understanding the data. A theoretical model of the dimer's energy states will be developed gradually as more background has been introduced. There will also be a discussion of the compound's crystal structure; these details will aid in the development of the theoretical model. Ultimately, the data for the magnetic properties of this compound will be presented and compared to calculations predicted by the theoretical model.

Chapter 1: Introduction

Magnetic effects of solid-state materials are largely attributed to how the electrons interact with each other and their lattice. The discovery of Schrodinger's equation allowed physicists to begin developing various quantum theories of solids to understand these interactions. Many models have since been created in an attempt to illustrate how the collective interactions of these electrons gave rise to macroscopic effects like conductivity or magnetization. To test the accuracy of these models, physicists would measure magnetic, and thermal transport properties of synthesized crystals and compare their data to the prediction of the theoretical models. As heavier atoms were introduced into the crystal making process, the number of electrons available to interact would consequently increase. This would ultimately require more complex models that were able to account for the multiple coupling effects.

Due to Pauli's exclusion principle, the number of electrons that may occupy an orbital is limited to two. This means that for systems with large numbers of electrons, it is necessary for the electrons to occupy orbitals with higher energy in order for the system to minimize its overall energy. The higher energy orbitals are more extended from the nucleus; thus, it is more likely for other interactions aside from coulombic repulsion to influence the system. Transition metal (TM) oxides composed of central ions whose valency lies in the $4d/4f$ orbitals, have enough distance between their neighboring ions so that certain exchange interactions may contribute in comparable magnitudes to that of the coulomb repulsion (*Table 1.1*) [3]. The relative magnitudes of these various interactions depend on the geometry of the solid, which in turn depends on the constituent atoms used to build it. Long-range magnetic ordering in solids containing these $4d/4f$ TM ions are determined by these interactions. Furthermore, the magnetic ordering of these solids is subject to change depending on various environmental factors like surrounding

temperature or the application of an external magnetic field. Many times, due to the complex geometries of the systems, predicting how the fundamental interactions give rise to magnetic order shifts become extremely difficult. This is also what makes materials synthesized with $4d/4f$ TM ions such fascinating candidates for research as new underlying physics to describe these systems can be discovered.

Electron Type	U (eV)	λ_{SO} (eV)	J_H (eV)	Interactions	Exemplary Phenomena
3*d*	5-7	0.01 – 0.1	0.7 – 0.9	$U >> J_H > \lambda_{SO}$	HTSC, CMR
4*d*	0.5 – 3.0	0.1 – 0.3	0.5 – 0.6	$U \sim J_H > \lambda_{SO}$	Orbital order
5*d*	0.4 – 2.0	0.3 – 1.0	~ 0.5	$U \sim J_H \sim \lambda_{SO}$	Novel J_{eff} = 1/2 state

Table 1.1. Displays the relative magnitude of various interactions as it relates to the number of electrons available in the system. [3]

The second chapter of this paper will introduce theories in condensed matter physics that guide in the construction of a theoretical model for $Ba_8NdRu_4Br_2O_{18}$. This will include exchange interactions, and crystal field splitting. The following chapter will contain brief overviews on the experimental techniques used to collect the data. Chapter four will be dedicated to analyzing the magnetic properties and crystal structure data collected. In chapter five, the theoretical model of the compound will be constructed and compared to the experimental data.

Chapter 2: Theoretical Background

2.1.1 Exchange interactions

The most logical topic to begin the theoretical background with is exchange interactions. Exchange interactions are largely concerned with the spin orientation of individual electrons and explain the mechanisms that give rise to magnetic ordering in solids. $Ba_8NdRu_4Br_2O_{18}$ contains transition metal ions with unfilled $4d$ and $4f$ shells. According to Hund's rule, the electrons in these shells will align themselves so that the total spin of the system is maximized [1]. This means that the electrons in the unfilled shell will orient their spins parallel to each other. Due to coulomb repulsion between electrons, it is more energetically favorable to fill the next degenerate state with an electron of the same spin rather than pair two together with opposite spin. Additionally, Pauli's exclusion principle tells us that no two electrons can occupy the same spin state if they occupy the same orbital. The electrons of partially filled TM ions can be regarded as identical fermions. The fact that these electrons are spatially close paired with the idea that they are indistinguishable is what motivates the adoption of exchange interactions.

If two electrons are bounded by some potential well, then their behaviors are described by a two-particle wave function that is anti-symmetric. This means that if the spatial wave function is symmetric, then the spin wave function must be anti-symmetric and vice versa. To differentiate between the two cases, it is common to refer to these wave functions in accordance to the coupling of their spin states

$$\psi_{Singlet} = \frac{1}{\sqrt{2}}[\psi_a(\boldsymbol{r}_1)\psi_b(\boldsymbol{r}_2) + \psi_a(\boldsymbol{r}_2)\psi_b(\boldsymbol{r}_1)]\chi_{Singlet}$$

$$\psi_{Triplet} = \frac{1}{\sqrt{2}}[\psi_a(\boldsymbol{r}_1)\psi_b(\boldsymbol{r}_2) - \psi_a(\boldsymbol{r}_2)\psi_b(\boldsymbol{r}_1)]\chi_{Triplet}$$

$\chi_{Singlet}$ refers to the coupled basis spin state of $|00\rangle$ while $\chi_{Triplet}$ corresponds to the states $|11\rangle$, $|10\rangle$, and $|1-1\rangle$. Now consider the Hamiltonian of the system with a first order perturbation that describes the coulomb repulsion between the electrons

$$\widehat{H} = \frac{p_1^2}{2m} + V(x_1) + \frac{p_2^2}{2m} + V(x_2) + \frac{e^2}{4\pi\epsilon_0 r}$$

Where $r = |\boldsymbol{r}(x_1) - \boldsymbol{r}(x_2)|$ and the perturbation is defined as $\widehat{H'} = \frac{e^2}{4\pi\epsilon_0 r}$. The energy of each couplet state is calculated by taking the expectation value of the Hamiltonian using the respective wave functions. Essentially, the perturbed Hamiltonian splits the ground state energy levels of the system according to the symmetry of the spin states. Taking the difference in energy between these states cancels out the zeroth order energy values yielding

$$E_{Singlet} - E_{Triplet} = 2\int \psi_a^*(\boldsymbol{r}_1)\psi_b^*(\boldsymbol{r}_2)\widehat{H'}\psi_a(\boldsymbol{r}_2)\psi_b(\boldsymbol{r}_1)d\boldsymbol{r}_1\, d\boldsymbol{r}_2$$

This difference of energies due to coulomb repulsion can be parameterized by the operator $\boldsymbol{S}_1 \cdot \boldsymbol{S}_2$, which motivates the construction of the following effective Hamiltonian

$$\widehat{H} = \frac{1}{4}\left(E_{Singlet} + 3E_{Triplet}\right) - (E_{Singlet} - E_{Triplet})\boldsymbol{S}_1 \cdot \boldsymbol{S}_2$$

It is necessary to define the exchange integral $J = \frac{E_{Singlet} - E_{Triplet}}{2}$ whose value determines the behavior of the exchange interaction taking place.

- If $J > 0$, then $E_{Triplet} < E_{Singlet}$ and the triplet spin state is favored leading to ferromagnetic ordering ($S = 1$).
- If $J < 0$, then $E_{Triplet} > E_{Singlet}$ and the singlet spin state is favored leading to anti-ferromagnetic ordering ($S = 0$).

When considering the exchange interactions effects of a many-body system the constant energy terms of the effective Hamiltonian can be ignored as the essential physics of the interaction is

determined by the spin dependent term. Thus, the exchange Hamiltonian of a many-body system can be written

$$\widehat{H}_{Exchange} = -2\sum_{i>j} J_{ij}\boldsymbol{S}_1 \cdot \boldsymbol{S}_2$$

Which accounts for spin interactions between all electrons within an atom.

2.1.2 Superexchange Interaction

The types of exchange interactions that can take place in a TM oxide largely depend on the geometry of the TM electron orbitals [3]. There is a type of exchange called direct exchange that occurs in overlapping electron orbitals. The overlapping in orbitals allows for a "direct" spin coupling effect between the electrons of neighboring atoms [1]. For TM oxides, the orbits of neighboring TMs are separated by an oxygen atom. Thus, direct exchange plays no effect between the coupling of neighboring TM ions; however, it serves as a precursor to understanding other types of exchange interactions.

The dominating exchange interaction that occurs in TM oxides is known as super exchange which is a type of indirect exchange. To understand this interaction, it is simplest to consider two TM ions containing one unpaired electron in each of their valence shells. In a TM oxide these two ions can be bounded at a 180º angle by an unmagnetized oxygen atom. The electrons of the oxygen atom can interact with the electrons of either TM ion due to an overlapping in orbitals, this is visually depicted in *Figure 2.1* [8].

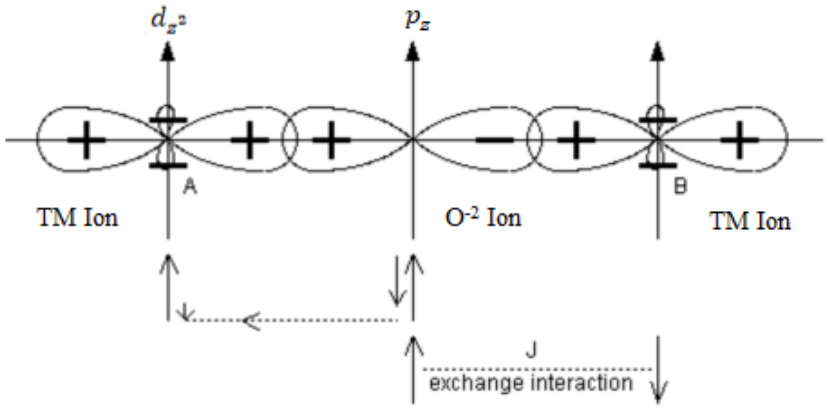

Figure 2.1. Illustration of the superexchange interaction in TM oxides. [8]

The interaction proceeds by an oxygen electron's spin directly coupling to the electron spin of a TM ion. In the figure, this is depicted by the left arrow connecting the O^{-2} spin down electron to the TM spin up electron (it is equally possible for the spin up electron of the O^{-2} ion to couple to a spin down TM ion leading to the same interaction in the reverse order). This leaves the left over spin up electron to couple with the other TM ion's electron, aligning it in the spin down orientation. Consider a chain of these bonds, at each subsequent TM ion site the spin orientation of the electron will be anti-parallel to the previous one.

The alignment of anti-parallel spin moments indicates anti-parallel magnetic moments over the solid and is known as antiferromagnetic ordering. Antiferromagnetic ordering in this geometric arrangement is favored as overall energy requirements are minimized. This model of geometric arrangement and magnetic ordering are more commonly seen in TM oxides; thus, it will come in handy when evaluating the magnetic order of $Ba_8NdRu_4Br_2O_{18}$ [1]. The alternative magnetic ordering scheme is known as ferromagnetic ordering and refers to the scenario where subsequent TM ion spins are parallel. This is most commonly seen when the TM-O-TM bond angel is at 90° and so, it will not be important for this paper.

2.1.3 Anisotropic Exchange Interaction

Another exchange interaction that plays a role in many TM antiferromagnets is the anisotropic exchange interaction. The spin-orbit coupling from a TM ion can lead to an exchange interaction between its excited state and a neighboring TM ion's ground state [3]. This interaction tends to have a stronger effect the lower the inversion symmetry of the crystal is, as the energy of the system depends on the magnetization direction. Named after the physicists who discovered it, Dzyaloshinsky and Moriya, the Hamiltonian is as follows

$$\widehat{H}_{DM} = \boldsymbol{D} \cdot \boldsymbol{S}_1 \times \boldsymbol{S}_2$$

Where $\boldsymbol{D}$ increases as inversion symmetry decreases. Due to the lack of symmetry, an orbital moment is produced that interacts with the spin of the unpaired TM electrons. In order to account for the local magnetic and orbital moments, neighboring electrons will cant their magnetic moments to minimize the energy of the system (*Fig. 2.2*) [3].

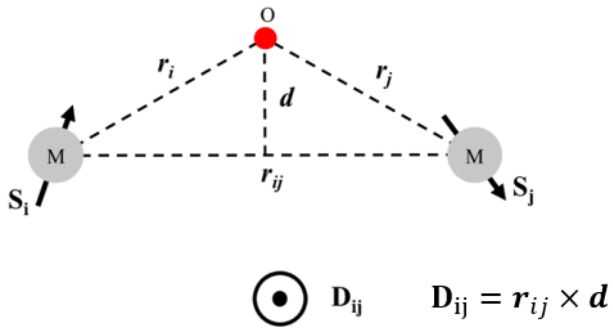

Figure 2.2. Visualization of Dzyaloshinsky-Moriya interaction. [3]

2.2.1 Crystal Field Splitting

Crystal field splitting is most accurate when applied to systems containing d orbital TM ions [1]. To understand how crystal field splitting works, it is first useful to consider a $4d$ TM ion's energy levels as they exist in a vacuum. The corresponding orbital magnetic quantum number for d is $l = 2$, meaning that the energy states of the d orbitals are 10-fold degenerate when considering spin. The goal of crystal field theory is to predict how these energy levels are affected by crystal environments. The symmetry of the crystal lattice serves as the determining factor for which energy levels are raised or lowered. Octahedral symmetry is the simplest environment to analyze energy level splitting for a TM ion, and happens to be a vital component to the dimer structure of $Ba_8NdRu_4Br_2O_{18}$. In an octahedrally symmetric cell, the TM will sit in the center of the shape while six oxygen atoms occupy the corners (*Fig. 2.3* (a)) [9].

The driving force behind energy splitting in the TM's d orbitals due to an octahedrally symmetric crystal environment is electrostatic repulsion from the neighboring oxygen atoms. To understand this splitting, it is first useful to categorize the d orbitals according to the alignment of their angular wave function. d orbitals whose angular wave functions lie along the x, y, or z axes are classified as e_g orbitals, and those that point between the cartesian axes are denoted t_{2g}

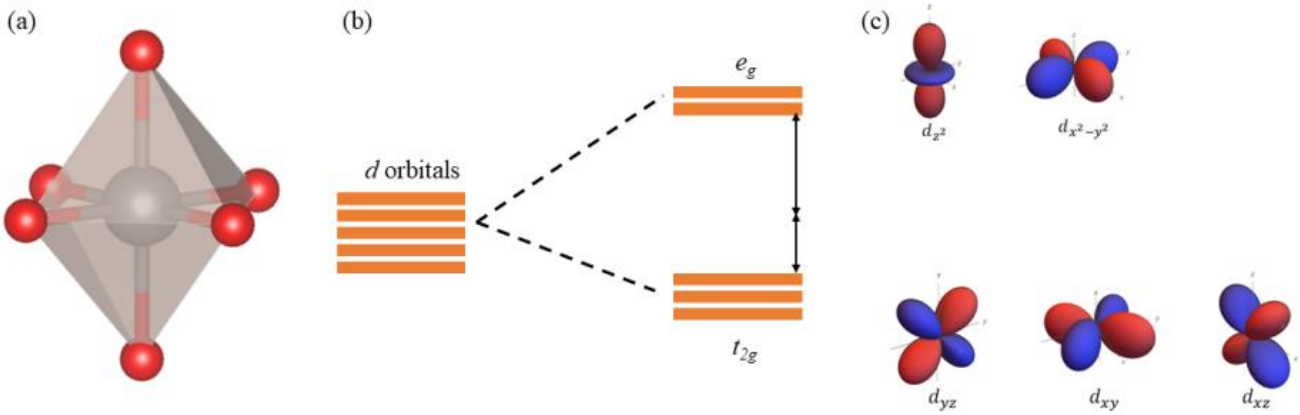

Figure 2.3. (a) Displays a transition metal oxide in an octahedrally symmetric local environment. (b) Energy splitting in the d orbitals due to a crystal environment. (c) Angular wave functions of d orbitals; energy of orbitals along axes are raised, while those that point away are lowered. [9]

orbitals (*Fig. 2.3* (c)). It is found that in an octahedral environment, the energies associated with e_g orbitals are raised while the energies of the t_{2g} orbitals are lowered [9].

The reason why e_g orbitals are raised and t_{2g} orbitals lowered can be understood when considering how these classes of orbitals interact with the surrounding oxygen orbitals. The $p-$ shell energy levels of the oxygen ion are occupied by at least one electron; furthermore, their angular wave functions lie along the cartesian axes. Since the t_{2g} orbitals don't point along the axes, there is no overlap between this set of TM d orbitals and the oxygen p orbitals. This in turn lowers coulomb repulsion effects, which leads to a lower energy requirement to occupy these states [1]. Consider a two-dimensional projection of the d_{xy} orbital (part of the t_{2g} orbitals) in the $x-y$ plane along with the p orbitals of the four oxygen atoms that are coplanar with the TM ion (*Fig. 2.4*).

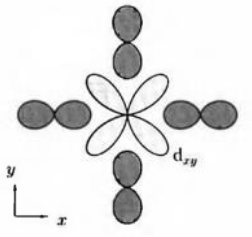

Figure 2.4. 2-D projection of d_{xy} orbital and oxygen p orbitals. [1]

Alternatively, the e_g orbitals do lie along the axes, leading to overlapping between the oxygen p orbitals and TM e_g orbitals. The overlapping of these orbitals leads to coulombic repulsion between the electrons of these orbits, increasing the energy required to occupy these states. The following two-dimensional image is built using the $d_{x^2-y^2}$ orbital; one of the two orbitals available for the e_g states (*Fig. 2.5*).

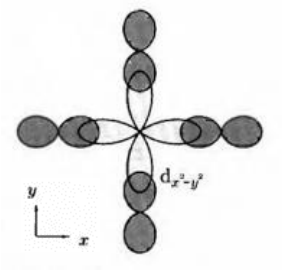

Figure 2.5. 2-D projection of $d_{x^2-y^2}$ orbital and oxygen p orbitals. [1]

When considering the energy splitting provided by an octahedrally symmetric field, filling the energy states is a more nuanced process compared to when there is no splitting. The orientation of electrons depends on the difference in energy between the split orbital states as they compare to the pairing energy [1]. To illustrate this idea, imagine that the crystally bound TM has six electrons in its d orbital. The first three electrons of the system can occupy each of the lowered t_{2g} states, orienting themselves in the spin up direction. The placement of the next electron is slightly ambiguous. Pairing energy refers to the energy cost of placing this fourth electron in one of the t_{2g} energy states with a spin down orientation. If this paring energy is less than the energy difference in e_g and t_{2g} states due to crystal splitting, then the electron will be placed spin down in one of the t_{2g} states. The remaining electrons will occupy the other available t_{2g} states in the spin down orientation so that the overall spin is minimized. This orientation of electrons is known as the strong-field case (*Fig. 2.6* (b)) [1]. The weak field case occurs when crystal splitting energy is smaller than the pairing energy, then e_g states will be occupied before pairing the final electron to a t_{2g} state (*Fig. 2.6* (a)). In 4d transition metal oxides the splitting energy is on the order of 2-5 eV which is typically larger than the pairing energy associated with these solids [3]. For this reason, many transition metal oxides are expected to be in the strong field orientation.

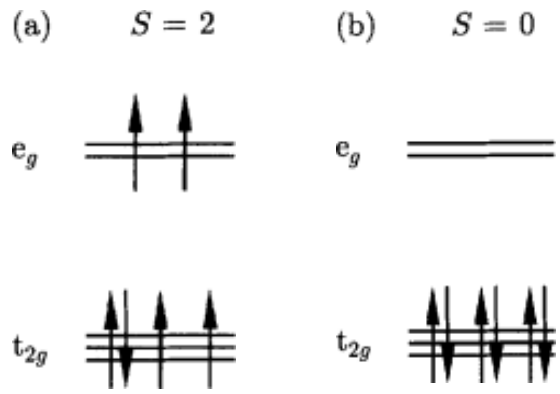

Figure 2.6. (a) High spin configuration due to weak field splitting (b) Low spin configuration due to strong field splitting. [1]

2.2.2 Trigonal Distortion

The e_g and t_{2g} states can be subject to further splitting if the geometry of the octahedron is distorted [9]. A distortion could be described as an elongation of the octahedron along one axis, the compression of the octahedron along opposite faces, or some other deformation of the original shape. Depending on the direction of the distortion applied to the octahedron, certain orbitals from the oxygen atoms will be displaced from their original positions allowing them to interact either more or less with the orbitals of the TM ion. The distortion most important for understanding properties of $Ba_8NdRu_4Br_2O_{18}$ is known as trigonal distortion and arises when face sharing dimers are formed [9].

Dimers are a type of structure built from two octahedrons where the two structures share either a corner, edge, or a face. It will be revealed in the discussion of crystal structure that $Ba_8NdRu_4Br_2O_{18}$ contains face sharing dimers. The distortion applied to the octahedrons of these dimers is a compressive force perpendicular to the plane of the shared face and arises from an attraction between the TM ions (*Fig. 2.7*).

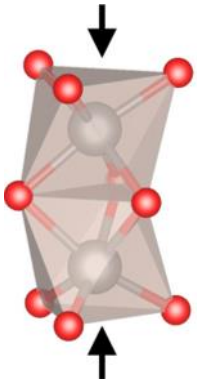

Figure 2.7. A visual showing the direction of compression for a trigonally distorted dimer. [9]

The t_{2g} orbit which points along the axis of distortion is raised in energy and relabeled as the a_{1g} orbital (*Fig. 2.8*). The remaining two t_{2g} orbitals are lowered in energy, as the distance to the closest oxygen p orbitals has been increased (renamed to e_g^{π} orbitals). Due to the crystal field splitting, the e_g orbitals can be neglected as there will not be enough electrons in the compound to occupy these states.

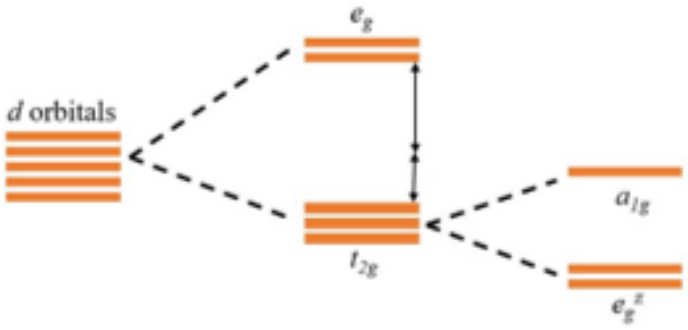

Figure 2.8. Energy level splitting due to trigonal distortion in the dimer. [9]

It must also be noted that in the process of forming the face sharing dimer that molecular orbits are formed between the TM ions. The bonding and anti-bonding molecular orbitals are depicted by combining the trigonally distorted energy levels of each TM octahedron (*Fig. 2.9*).

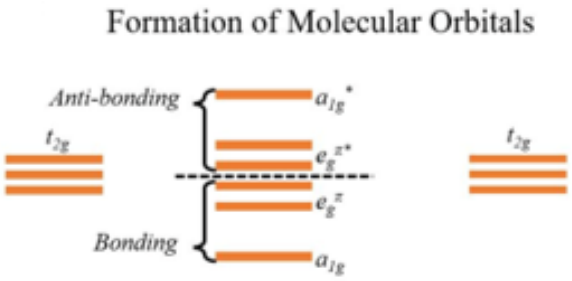

Figure 2.9. Formation of Molecular orbits in a trigonally distorted dimer. [9]

This diagram of energy levels will be used to calculate the theoretical magnetic moment of the dimer lattice, and thus is vital to the framework of the theoretical model.

Chapter 3: Research Methods

3.1 Energy Dispersive X-Ray Analysis

The first step of analyzing the properties of a crystal once it has been synthesized is confirming the synthesis produced the desired crystal. The composition of a compound can be estimated using energy dispersive x-ray analysis (EDX). The EDX machine shoots energized electrons at the crystal sample. Incident electrons can knock loose the electrons that lie within inner shells of an atom, initiating an outer electron to fill the vacancy. In the process of an outer electron lowering its energy it emits an x-ray at some discretized frequency corresponding to the energy drop (*Fig. 3.1*). The various x-rays emitted through this process are counted and matched to the energy spectrums of the various constituent atoms to determine the overall composition.

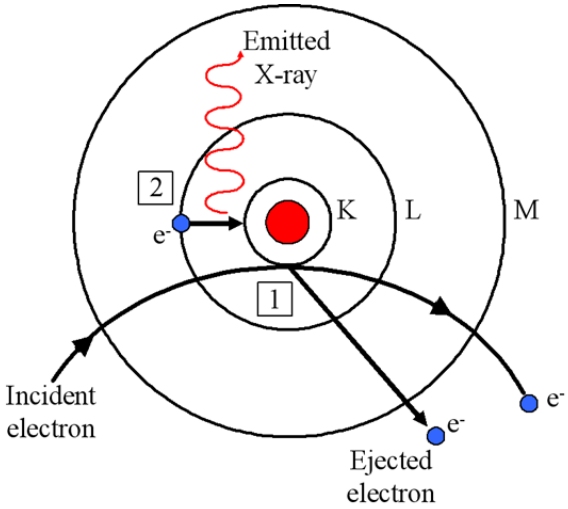

Figure 3.1. Displays how EDX collects data (1) Incident electrons knock loose an inner shell electron (2) Electron from outer shell drops in energy to fill the vacancy by emitting an x-ray. The x-rays emitted are then counted by a detector. [6]

3.2 Magnetic Property Measurements

In order to gain a deeper understanding of the coupling effects that can dictate a compounds behavior, the various transport properties must be measured. Transport properties can be measured by attaching leads to a sample and running a current through the crystal to measure voltage differences due to some independent variable. By varying the temperature of the environment, or applying a magnetic field to the crystal the conductivity can be described as a function of the independent variable being tested. Unfortunately, the sample sizes in the batch of $Ba_8NdRu_4Br_2O_{18}$ used for this project were too small to attach leads to, and measure transport properties effectively. Thus, this paper will focus solely on comparing the measured magnetic properties of the material to the predictions of the theoretical model.

Magnetic Property Measurement System

The magnetic properties of materials are measured using a magnetic property measurement system (MPMS). The primary mechanism within the MPMS that results in accurate measurements of these properties is the supercooled quantum interference device (SQUID). Utilizing a combination of quantum mechanical phenomena is what allows for the SQUID to serve as such an accurate magnetometer [2]. SQUIDs are superconducting rings that contain Josephson junctions at opposite ends of the ring (*Fig. 3.2*). The Josephson junctions can be regarded as insulating barriers and will be discussed in greater detail.

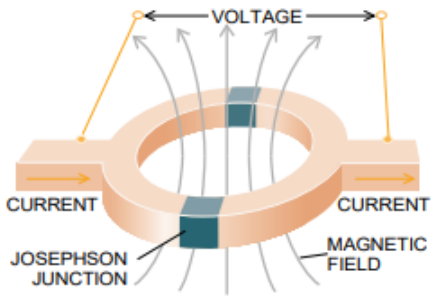

Figure 3.2. Illustration of a SQUID. [2]

In supercooled materials, electrons move together in what are known as Cooper pairs. Cooper pairs consist of two electrons with opposite spin and momentum. As one electron moves through the lattice it attracts the ions, pulling them physically closer and producing an area of greater positive charge density [2]. The second electron is then attracted to this region of charge density, allowing it to move behind the first electron continuously throughout the lattice [2]. In typical conductor's, the vibrational modes of ions prevent this effect from happening and instead the free electrons experience random motion, otherwise known as resistance.

Another quantum mechanical phenomenon vital to the operation of the SQUID is the Josephson effect. This effect occurs at the junction of two superconductors separated by an insulating barrier. Brian Josephson found that if the insulating barrier was sufficiently small, that cooper pairs could tunnel to the other side while retaining their coupled wave function [2]. The critical current refers to the maximum current that can flow across a Josephson junction before cooper pairs are decoupled. When the current applied to a SQUID exceeds the critical current, a voltage is produced across the SQUID [2]. Since the SQUID is built in a ring shape, a magnetic flux can be passed through its center, leading to a raising or lowering in the value of the critical current [2]. These various effects can be exploited to detect very minor changes in voltage across the SQUID.

To measure the properties of a material, a sample is pulled through a series of detection coils that have a magnetic field running through them. A current will form in the detection coils in a direction that appropriately counters the magnetic flux they experience. This current is then passed through an input coil in order to reconvert the energy back into a magnetic field (*Fig. 3.3*). It is this magnetic field produced by the input coils that is detected by the SQUID, effectively converting magnetic flux into voltage. As the sample is pulled through the coils its

influence on the gradient of the magnetic field is detected by the SQUID. This information is then converted into magnetization data for the material through the MPMS software. There are a variety of functions that the MPMS can perform in order to extract magnetization data. The data measured from this device will be introduced and analyzed in chapter four.

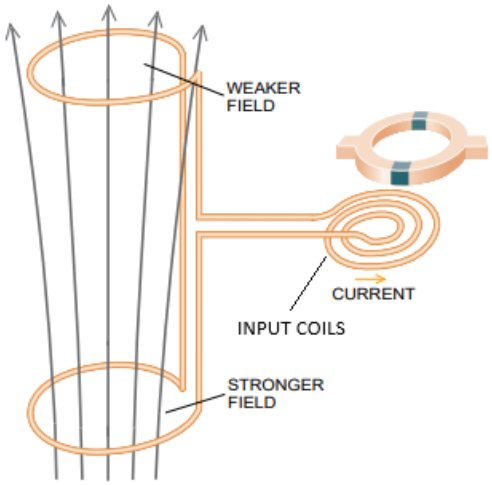

Figure 3.3. Illustration of the MPMS magnetometer. [2]

3.3 X-Ray Diffraction

The geometries of crystals can be categorized into seven crystal systems which collectively can be split further into 230 space groups depending on the symmetries of the crystal structure. Understanding these symmetries aids in developing a model capable of predicting magnetic properties. The geometries of crystal structures can be unraveled using an x-ray diffraction (XRD) machine. To understand how XRD works it is important to first discuss Bragg's Law, which is defined as follows

$$2d \sin\theta = n\lambda$$

Consider a beam of radiation incident upon a crystal with parallel lattice planes at an angle θ. If the distance between consecutive lattice planes is defined as d then the path difference of reflected rays by adjacent planes is $2d \sin\theta$ (*Fig. 3.4*) [5]. Constructive interference peaks occur

when the incident angle is equal to the angle of scattering. When this happens, the path difference will be equal to some integer number n multiplied by the wavelength λ of the incident beam. The x-ray diffraction machine operates using Bragg's law, and tracks the angle at which scattered intensity peaks are measured. X-rays are in the ideal frequency range to penetrate through layers of crystal [5]. By measuring these refraction peaks along different angles of the crystal, the various lattice spacings d can be determined. Applying a Fourier transform to this set of data maps the real space lattice to the reciprocal space lattice where its geometry can be defined using space groups.

To solve the structure of $Ba_8NdRu_4Br_2O_{18}$ an x-ray of wavelength 0.71073 Å was scattered along different planes of the crystal. After one scan across a single plane, the crystal system of the lattice can effectively be determined. Depending on the symmetry of the system, the machine will draft another set of scans across various planes of the crystal. The lower the symmetry of the crystal the more scans will be needed to produce an accurate structure. After the scans across all planes have been completed, the images of all the diffraction peaks are processed to integrate detections of the same peak along different axes into one image. From here, the space group can be determined which allows for further analysis of the structure.

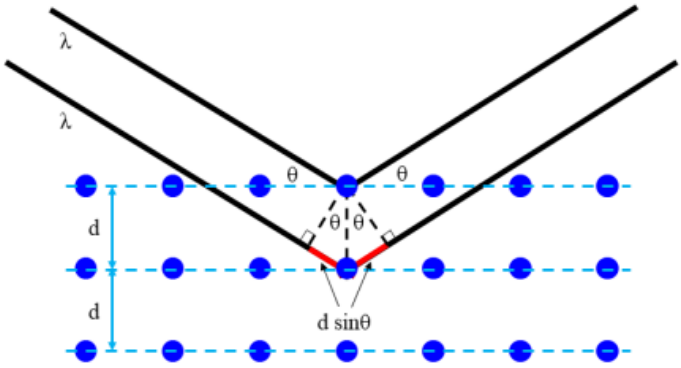

Figure 3.4. A visual to aid in understanding Bragg's law. [5]

The XRD machine gives details about the charge densities at various locations of the crystal, which are used to make educated predictions of where the constituent atoms lie within the lattice. The space group is modeled in a program where different atoms can be placed at the charge densities corresponding to the space group's symmetry. The properties of this virtual structure are cross referenced against the data collected from XRD to see if the theoretical structure is correct. As the accuracy of the theoretical structure increases the R1 number will decrease. Once this number reaches a value of ≤ 0.15, the theoretical model is accepted as being accurate. The only way to reduce the R1 number would be to reach better approximations for the unit cell lengths; however, the impacts these corrections have on the physics of the system are negligible in the context of this paper.

Chapter 4 Data & Analysis

4.1 EDX Data

The EDX data for $Ba_8NdRu_4Br_2O_{18}$ is shown below (*Fig. 4.1*)

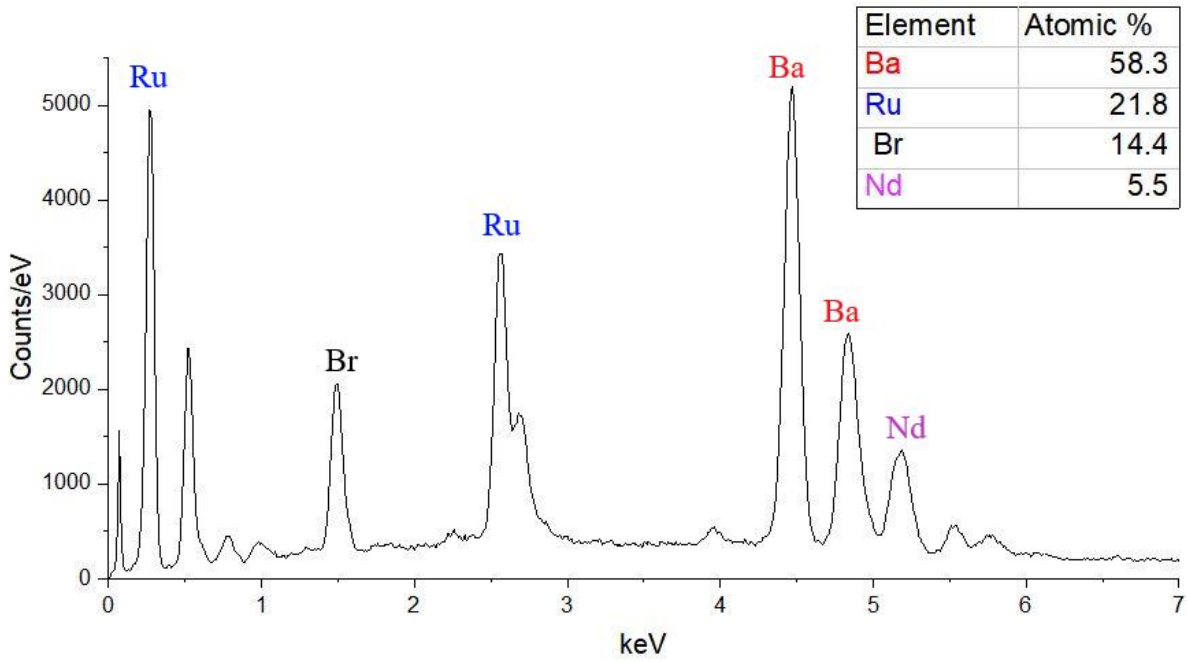

Figure 4.1. Displays EDX data for $Ba_8NdRu_4Br_2O_{18}$.

The EDX data suggests that the sample used does not contain the desired compositions of each element. This is likely due to the fact that the elements of this compound share frequencies in their energy spectrums. For example, the ratio of Ba:Ru is slightly lower than expected while the ratio of Ba:Nd is slightly higher than expected. Ruthenium and neodymium atoms share energy spectra around 500 eV; thus, ruthenium was receiving counts for x-ray detections when they should have been attributed to neodymium. Furthermore, the relative composition of oxygen within the substance was not measured. Earth's atmosphere contains a significant enough presence of oxygen that readings for this atom are likely to be skewed. Nevertheless, the relative composition of elements, combined with the understanding that data may be slightly skewed due

to energy spectra overlap instils enough confidence to proceed with the sample. Anyhow, the details of the compound's composition are clarified when solving the XRD data for structure.

4.2 XRD Data

From the first XRD scan, it was determined that $Ba_8NdRu_4Br_2O_{18}$ had trigonal symmetry with rhombohedral crystal centering. After completing twelve more scans and running the necessary integration and refinement programs, the structure of the compound was solved with a $R-3$ space group achieving an R1 number of 0.1307. The structure was extremely complex, and so in order to solve its geometry in an efficient way, structure data for its parent compound $Ba_8Ru_5Br_2O_{18}$ was referenced (*Ref.* [4]). *Figure 4.2* provides a comparison of these two compounds unit cells, where the ruthenium octahedron of the parent compound is replaced by a neodymium octahedron. Using the published data as a blueprint, the most difficult aspect of solving this doped structure became finding the placement of the neodymium ion.

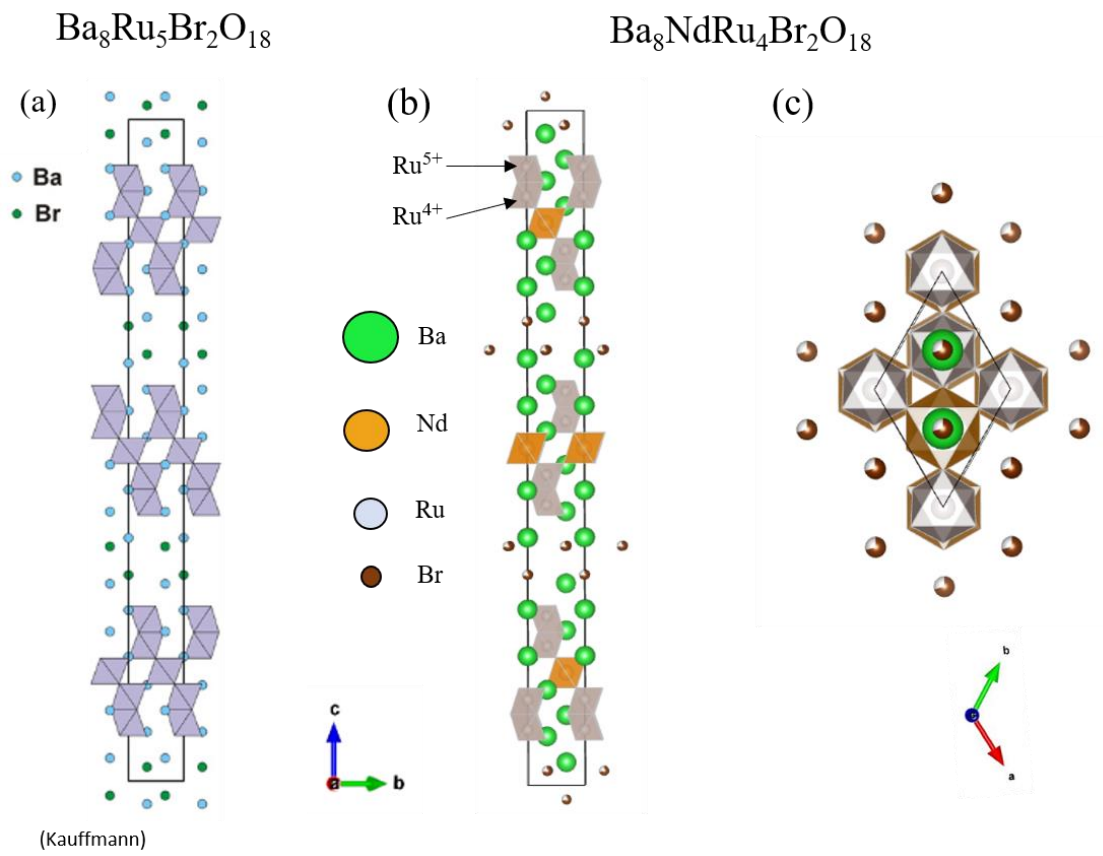

Figure 4.2. (a) Structure of the parent compound $Ba_8Ru_5Br_2O_{18}$. (b) Structure of the studied compound $Ba_8NdRu_4Br_2O_{18}$. (c) Looking down the c direction of the studied structure. [4]

In TM oxides, the physics of the materials are largely attributed to how the TM interacts with their environment, often the other constituent atoms serve as structural support for the crystal. Thus, to understand what gives rise to a magnetic TM oxide's magnetic properties and long-range ordering, it is practical to focus on the physics of the TM's local environment. The structure data of $Ba_8NdRu_4Br_2O_{18}$ indicated that in one formula unit, there exists two dimers composed of ruthenium, and one neodymium octahedron. The neodymium ion used to build this compound has a partially filled $4f$ orbital. For this reason, the neodymium octahedron provides contributions to the material's magnetic properties at comparable magnitudes to the ruthenium dimers. In order to develop a model for this compound's ground state that can effectively make predictions, both of these structures must be accounted for. The compounds crystal structure data

was the only ingredient used to build the theoretical model. Predictions from this model are contrasted against the magnetization data to test its accuracy.

4.3 Magnetization

The relationship between magnetic susceptibility χ and magnetization M of a material is defined as

$$M = \chi H$$

Where H is an applied magnetic field. Materials composed of atoms with unpaired electrons are defined as magnetic materials. In magnetic materials, it is possible for the symmetries pertaining to magnetically ordered states to break when a sufficiently high temperature of the material has been reached. As a result of symmetry breaking, the dipole moments of neighboring atoms will randomly align themselves, and the material is considered to be paramagnetic. In a paramagnetic state, Curie-Weiss fitting can be performed on the magnetization data to determine the Curie constant C [7].

$$\chi = \frac{C}{T - \theta_{CW}}$$

The Curie constant can be used to calculate the effective dipole moment of one formula unit in the paramagnetic state with

$$\mu_{eff} = 2.828\sqrt{C}$$

The Curie-Weiss temperature is defined by the constant θ_{CW}, whose value determines the temperature (in kelvins) at which magnetic ordering symmetries break. For antiferromagnets the value of $\theta_{CW} < 0$ and must be multiplied by negative one to extract physical meaning [7].

The MPMS can perform two functions: a magnetic field sweep, and a temperature sweep. The temperature sweep determines magnetization as a function of temperature at some constant

field strength; the field sweep measures magnetization as a function of an applied magnetic field at some constant temperature.

4.3.1 Temperature Dependence of Magnetization

In the temperature sweep, the applied magnetic field was kept at 0.2 T and the temperature varied from $\sim 0\ K - 350\ K$. In *Fig. 4.3* the raw magnetization data along the ab direction is displayed in black.

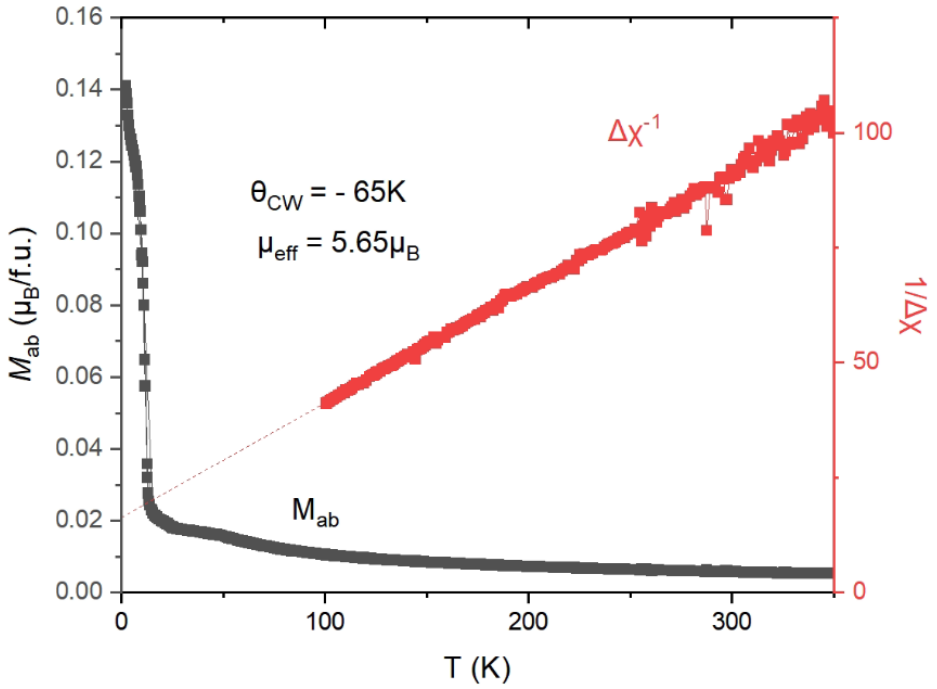

Figure 4.3. Magnetization data for a temperature sweep along the ab – direction.

A Curie-Weiss fit was performed on the raw data to obtain the red line, whose slope is defined by the Curie constant. For this set of data $C = 4$ and so the $\mu_{eff} = 5.65\mu_B$ where the Bohr magneton is defined as $\mu_B = \frac{e\hbar}{2m_e}$. It was also found from the Curie-Weiss fitting that

$\theta_{CW} = -65\ K$. Since $\theta_{CW} < 0$ this indicates anti-ferromagnetic ordering in the ab direction, below the negation of the Curie-Weiss temperature.

Magnetization along the c direction was also measured with the same constants and independent variables used along ab.

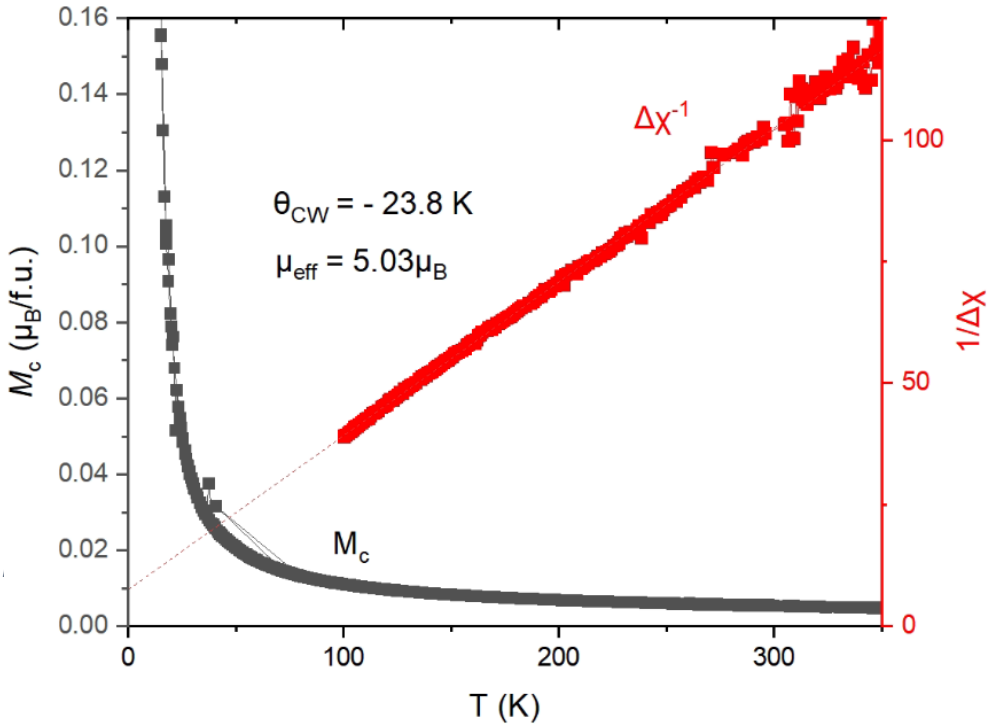

Figure 4.4. Magnetization data for a temperature sweep along the c – direction.

Curie-Weiss fitting along this directions data produced a Curie constant $C = 3$ from which an effective magnetic moment was calculated $\mu_{eff} = 5.03\mu_B$. Similar to the ab direction, the Curie-Weiss temperature along c is also negative. Thus, antiferromagnetic ordering can be expected along this direction as well.

The theoretical model will not be complex enough to specify direction of magnetic moment. To test its accuracy, the theoretically predicted value for effective magnetic moment will be compared to the average of the effective magnetic moments along ab and c. The average effective moment is calculated to be $\mu_{eff}^{avg} = 5.34\mu_B$. Also, it must be noted that the Curie-Weiss

temperature of this compound suggests that the super exchange interaction is responsible for the anisotropic magnetic ordering.

4.3.2 Magnetic Field Sweep Data

When measuring magnetization as a function of applied magnetic field, the temperature of the crystal was held constant at $2\ K$. The field strength applied to the crystal varied from $0 - 7\ T$. This relationship was measured along both axes (ab and c) to see if there were any discrepancies. The data from each of the runs are both plotted on the same graph below.

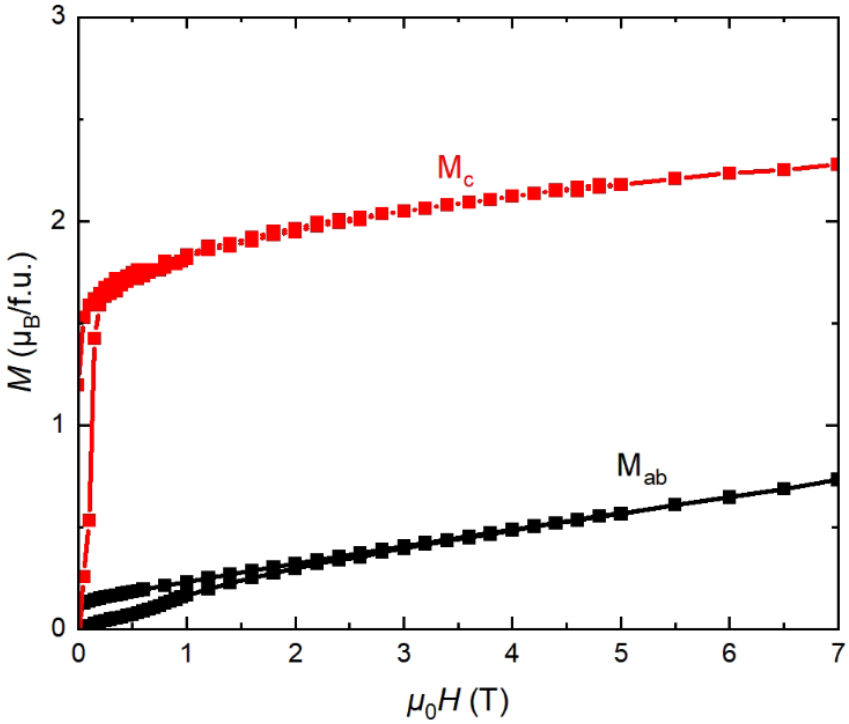

Figure 4.5. Magnetization data for a magnetic field sweep along both the ab, and c directions.

As the magnetic field increases, the magnetization along c is much greater than it is in the ab direction. This indicates that the material has anisotropic dipole moments, a result of the Dzyaloshinsky-Moriya interaction. The c direction is considered the "easy axis" as magnetization along this direction is greater. Similarly, the ab direction is considered the "hard axis". Furthermore, a split in each of the data sets can be seen near the origin. When conducting

the field sweep, the MPMS was instructed to continue measurements as the magnetic field was reduced from 7 to 0 T. Typically, the bottom line corresponds to data measured when the applied magnetic field increases, and the top line corresponds to data measured in a decreasing magnetic field. The important thing to understand from this behavior is that magnetic order shifts for this compound depend on the history of the material. This is known as magnetic hysteresis, and although this phenomenon isn't predicted in the theoretical model it is a property of the material that deserves mention.

Chapter 5: The Theoretical Model

The energy diagrams developed in chapter two as a result of crystal field splitting and trigonal distortion serve as a blueprint for the theoretical model. As previously stated, the physics of the neodymium octahedron must be considered in addition to the two ruthenium dimers. The Nd^{+3} ion contains one unpaired electron in its 4f shell. Since the 4f orbital wavefunction is delocalized, the crystal splitting terms become less important than the spin orbit coupling. The energy diagram won't be required; instead, the effective moment of this octahedron can be solved using the term symbol for Nd^{+3} and the following equation

$$\mu_{eff} = g_J \mu_B \sqrt{J(J+1)}$$

Where g_J is the Landé g-value for some value of angular momentum J. For the neodymium octahedron $g_J = .72$ and the $\mu_{eff} = 3.62\mu_B$.

For the ruthenium dimers, constructing an energy diagram aids tremendously in determining the effective moment of the structure. To begin filling a trigonally distorted dimer energy diagram, the number of electrons available must first be determined. In order for one formula unit of the compound to have neutral charge, each ruthenium atom must have a charge of $+4.75$ (*Fig. 5.1*).

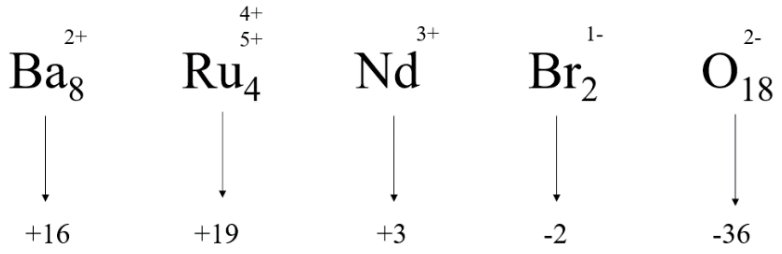

Figure 5.1. Visual to aid in determining the average charge per ruthenium ion.

This number was determined by dividing the charge required by the ruthenium atoms to neutralize the compound, by the number of available ruthenium atoms in one formula unit. This average charge per ruthenium atom can be obtained if one dimer is composed of two Ru^{+5} ions and the other of one Ru^{+5} and one Ru^{+4} ion. For each dimer there will be a corresponding strong and weak field case for the spin arrangements. All possible combinations of spin states between the two dimers and neodymium octahedron will be tested to see which one produces an effective moment closest to the experimentally determined value.

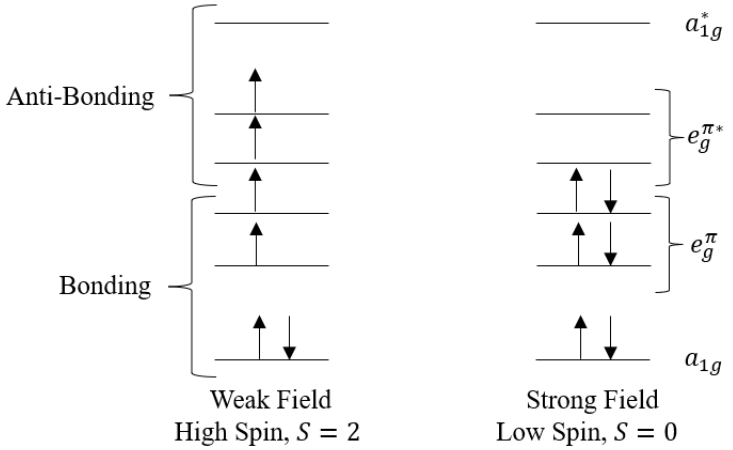

Figure 5.2. Possible spin orientations of the Ru^{5+}/Ru^{5+} Dimer.

The above figure displays the possible spin state arrangements in the dimer containing two Ru^{+5} ions (*Fig. 5.2*). To calculate the effective moment of these dimers, the angular moment is assumed to be $L = 0$ for simplicity. Thus, the equation for effective magnetic moment becomes

$$\mu_{eff} = 2\mu_B\sqrt{S(S+1)}$$

Where $g_J = 2$. Using this equation, the effective moments of the weak and strong field cases for this dimer are $\mu_{eff} = 4.90\mu_B$ and $\mu_{eff} = 0$ respectively.

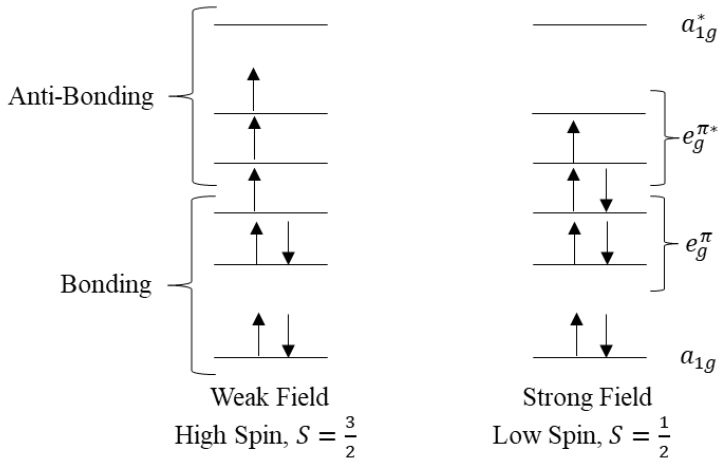

Figure 5.3. Possible spin orientations of the Ru^{5+}/Ru^{4+} Dimer.

Next, the effective moments of the potential formations for the Ru^{+4}/Ru^{+5} dimer must be calculated (*Fig. 5.3*). Using the same equation, the moments of the weak and strong field cases are $\mu_{eff} = 3.87\mu_B$ and $\mu_{eff} = 1.73\mu_B$ respectively. Since there are two dimers with two potential spin orientations each, there are four possible combinations that must be tested. It is also necessary to include the effective moment of the neodymium octahedron when testing these combinations. The average effective moment of one formula unit based on the theoretical model is calculated using a quadrature sum. When combining a Ru^{+4}/Ru^{+5} dimer in the weak field state, with a Ru^{+5}/Ru^{+5} dimer in the strong field state, (while also accounting for the neodymium octahedron) an effective moment of $\mu_{eff} = 5.30\mu_B$ is calculated. Out of the possible combinations, this one produced a value for the effective moment that was closest to the experimentally determined one ($\mu_{eff}^{avg} = 5.34\mu_B$).

The theoretical model considers the magnetic dipole moments of a neodymium octahedron and two dimers composed of ruthenium ions. Energy diagrams used to calculate the magnetic moments are determined by the geometry of the crystal lattice. From these calculations, it was established that the dimer containing the Ru^{+4} ion needed to be in the low spin orientation

while the Ru^{+5} dimer takes the high spin state, to acquire the most accurate value for effective magnetic moment. The low spin orientation is typically what is predicted for magnetic transition metal oxides by condensed matter theories used today. Many of these theories such as crystal field theory are built under the assumption that the crystal lattice contains a high degree of symmetry. As the symmetry within a crystal lattice disappears, predictive capabilities of these theories tend to be reduced. It is very likely that the complex symmetry within the $Ba_8NdRu_4Br_2O_{18}$ crystal lattice makes it so that a high spin orientation in the Ru^{+5} dimer is more energetically favorable.

Conclusion

Overall, the theoretical model came close to predicting the effective magnetic moment of the paramagnetic state. Using this model, the effective moment of the system was calculated with $\%\ error = \sim 0.75\%$. Furthermore, the theoretical model permits the existence of Dzyaloshinsky-Moriya interactions and can visually depict the super exchange interaction. Aside from these positives the model is still technically incomplete. As previously mentioned, due to the extremely small crystals of this sample it was not possible to collect reliable transport data. Had this data been collected, further insights into the behavior of the material could be made. This includes but is not limited to, transitions from conducting to insulating states, and information regarding the compounds heat capacity. If further investigations were to be conducted on this material, collecting thermal and magnetic transport data would be prioritized. Additionally, neutron scattering is an experiment that determines the magnetic dipole moment of each atom within a compound. Having access to this data would allow for more precise calculations regarding spin canting, resulting in a deeper understanding of the Dzyaloshinsky-Moriya interaction taking place. The goal of this project was to understand magnetic properties

of $Ba_8NdRu_4Br_2O_{18}$ using a theoretical model. Altogether, the theory developed proved to be successful in achieving predictive capabilities in the paramagnetic state.

Bibliography

[1] Blundell, Stephen John. *Magnetism in Condensed Matter*. Oxford University Press, 2014.

[2] Clarke, John. "SQUIDs." *Scientific American*, vol. 271, no. 2, Aug. 1994, pp. 46–53.

[3] G. Cao and L. DeLong, Physics of Spin-Orbit-Coupled Oxides (Oxford University Press, 2021).

[4] Kauffmann, Matthieu, et al. "Layered Ruthenium Hexagonal Perovskites: The New Series [ba2br2−2x(co3)x][Ban+1runo3n+3] with n=2, 3, 4, 5." *Journal of Solid State Chemistry*, vol. 180, no. 7, July 2007, pp. 1957–1966.

[5] Kittel, Charles. *Introduction to Solid State Physics*. 8th ed., John Wiley & Sons, 2004.

[6] McAneney, Jonny. (2005). Characteristics of Thin and Ultrathin Ferroelectric Capacitor Structures.

[7] Mugiraneza, Sam, and Alannah M. Hallas. "Tutorial: A Beginner's Guide to Interpreting Magnetic Susceptibility Data with the Curie-Weiss Law." *Communications Physics*, vol. 5, no. 1, 2022.

[8] Suzuki, Masatsugu Sei. *Superexchange Interaction*. Binghamton University, 28 May 2009.

[9] Zhao, Hengdi, and Gang Cao. "Discovery and Control of Quantum States in 4D/5D Transition Metal Materials."